# Feasibility study for using an extended three-wave model to simulate plasma-based backward Raman amplification in one spatial dimension

T.-L. Wang,[1] D. Michta,[2] R. R. Lindberg,[2,3] A. E. Charman,[2] S. F. Martins,[1] and J. S. Wurtele[2,4]
[1]*Department of Electrical Engineering, University of California at Los Angeles, Los Angeles, California 90024, USA*
[2]*Department of Physics, University of California at Berkeley, Berkeley, California 94720, USA*
[3]*Argonne Accelerator Institute, Argonne National Laboratory, Argonne, Illinois 60439, USA*
[4]*Center for Beam Physics, Lawrence Berkeley National Laboratory, Berkeley, California 94720, USA*

(Received 17 August 2009; accepted 7 December 2009; published online 30 December 2009)

Results are reported of a one-dimensional simulation study comparing the modeling capability of a recently formulated extended three-wave model [R. R. Lindberg, A. E. Charman, and J. S. Wurtele, Phys. Plasmas **14**, 122103 (2007); Phys. Plasmas **15**, 055911 (2008)] to that of a particle-in-cell (PIC) code, as well as to a more conventional three-wave model, in the context of the plasma-based backward Raman amplification (PBRA) [G. Shvets, N. J. Fisch, A. Pukhov *et al.*, Phys. Rev. Lett. **81**, 4879 (1998); V. M. Malkin, G. Shvets, and N. J. Fisch, Phys. Rev. Lett. **82**, 4448 (1999); Phys. Rev. Lett. **84**, 1208 (2000)]. The extended three-wave model performs essentially as well as or better than a conventional three-wave description in all temperature regimes tested, and significantly better at the higher temperatures studied, while the computational savings afforded by the extended three-wave model make it a potentially attractive tool that can be used prior to or in conjunction with PIC simulations to model the kinetic effects of PBRA for nonrelativistic laser pulses interacting with underdense thermal plasmas. Very fast but reasonably accurate at moderate plasma temperatures, this model may be used to perform wide-ranging parameter scans or other exploratory analyses quickly and efficiently, in order to guide subsequent simulation via more accurate if intensive PIC techniques or other algorithms approximating the full Vlasov–Maxwell equations.
 [doi:10.1063/1.3280012]

## I. INTRODUCTION

While warm and cold fluid models certainly find many applications in numerical plasma simulation, the capability to incorporate true kinetic effects may be essential in the simulation of certain laser-plasma interactions. One of the main tools used in this effort has been the particle-in-cell (PIC) family of algorithms, in which the plasma is modeled as a system of discrete macroparticles that move according to both external and self-consistent electric and magnetic fields calculated on a spatial grid using interpolated sources, and then in turn interpolated back to the particle positions.[1] PIC codes may be interpreted as numerical approximations to the full Vlasov-Maxwell equations, using mixed Eulerian/Lagrangian spatial discretizations for the fields and sources combined with quasirandom Monte Carlo representations for the plasma momentum distribution function, and are considered the current state-of-the-art in numerical modeling of ideal plasma kinetic theory, having benefited from a relatively extensive and productive period of development and refinement implementing various numerical techniques to make the simulations more robust against spurious collisionality and other sources of particle and grid noise.

However, the nature of PIC simulations makes them computationally intensive, sometimes requiring, even in one-dimensional (1D) spatial geometry, the use of millions of cells and tens of millions of macroparticles in order to adequately resolve the laser wavelengths and fine-scale plasma wave structure. (Of course, alternative "direct" phase-space methods for the solution of the Vlasov equation can be equally expensive computationally in 1D, and even worse in higher dimensions.) One particular case for which the computational requirements are rather demanding is the simulation of the plasma-based backward Raman amplification (PBRA) problem.[2–4] For such scenarios, the PIC cell size must resolve the laser beat wavelength, while the simulation size must be comparable to the full length of the plasma; typically the ratio of these scale lengths is of order $\gtrsim O(10^4)$. Therefore it is of practical interest to employ an alternative reduced description which can run much faster than PIC algorithms yet still incorporate with some accuracy and fidelity the most important underlying kinetic effects present in PBRA or similar laser-plasma interactions but which cannot be captured by standard fluid theories. In this paper we carry out a preliminary comparison between 1D simulation results of PBRA from an extended three-wave (ETW) model formulated by Lindberg *et al.*[5,6] and from a standard PIC code, as well as from a more conventional three-wave model that includes only linear kinetic effects in the plasma wave dynamics.

The remainder of the paper is organized as follows. In Sec. II we briefly discuss the underlying theory of the ETW model and describe its particular features. In Sec. III we compare the results of a 1D PBRA case study in which plasmas of different electron temperatures are simulated using PIC and ETW algorithms, as well as with an even simpler

 

three-wave model without nonlinear kinetic corrections that provides numerical "control" runs to better evaluate the merits and limitations of the extended model. In Sec. IV we summarize and assess the results and mention possibilities for future development of the ETW or related models.

## II. EXTENDED THREE-WAVE MODEL DESCRIPTION

Three-wave (or more generally, multiwave) models arise in many physical settings as simple and efficient means for describing the wave energy and action exchange between coupled modes of a collective system and are commonly employed to describe the essential physics of Raman scattering, Brillouin scattering, or other parametric instabilities in plasmas. We seek a simple extension of the usual three-wave model for Raman interactions in underdense, nonrelativistic plasma in one spatial dimension, which retains much of the computational simplicity and efficiency but includes dominant kinetic effects, manifesting as linear and nonlinear damping and detuning of the Langmuir wave.

For the specific case of PBRA, the three modes of interest are given by the pump laser field, a counter-propagating seed laser field, and a Langmuir wave, with the goal being efficient energy transfer from the long pump mode into the short seed mode, mediated by the plasma mode, via coherent Raman scattering, whereby the beating EM waves induce transverse quiver on plasma electrons and ponderomotively force the plasma wave, whose quasiperiodic density perturbations in turn act as an effective grating which can further scatter EM energy between the laser modes.

To describe PBRA as an interaction among three nearly harmonic waves, we make an eikonal assumption, or slowly varying envelope approximation for all waves, decomposing each of the complexified laser and plasma fields into a complex amplitude, or envelope, modulating a sinusoidal carrier oscillation characterized by a real phase, and presuming that any variations of the amplitude occur over spatiotemporal scales that are much longer/slower than the rapid advance in the phase. Thus, we express the (assumed) circularly polarized, Coulomb-gauge, laser vector potential (in Gaussian units) as a superposition of pump and seed contributions, written in terms of the normalized pump laser envelope $a_0(z,t)$ and seed laser envelope $a_1(z,t)$ and the corresponding pump phase $\phi_0(z,t) \equiv -k_0 z - \omega_0 t$ and seed phase $\phi_1(z,t) \equiv k_1 z - \omega_1 t$, for some choice of real, positive carrier frequencies $\omega_{0,1}$ and wavenumbers $k_{0,1}$:

$$\mathbf{A}(z,t) = \frac{m_e c^2}{e\sqrt{2}}[a_0(z,t)e^{-i(k_0 z+\omega_0 t)} + a_1(z,t)e^{+i(k_1 z-\omega_1 t)}]\hat{\boldsymbol{e}}_+ + c.c. \equiv \frac{m_e c^2}{e\sqrt{2}}[a_0 e^{i\phi_0} + a_1 e^{i\phi_1}]\hat{\boldsymbol{e}}_+ + c.c., \quad (1)$$

where $e$ is the magnitude of the elementary electric charge, $m_e$ is the electron mass, $c$ is the speed of light *in vacuo*, $\hat{\boldsymbol{e}}_\pm = \hat{\boldsymbol{e}}_\mp^* = (\hat{\boldsymbol{x}} \pm i\hat{\boldsymbol{y}})/\sqrt{2}$ denote the circular-polarization basis vectors, and we assume that $|\partial_t a_{0,1}| \ll \omega_{0,1}|a_{0,1}|$ and $|\partial_z a_{0,1}| \ll k_{0,1}|a_{0,1}|$ throughout the evolution, such that the envelopes are slowly varying compared to the corresponding carrier oscillations.

Similarly, we express the longitudinal electrostatic field $E_z(z,t)$ of the plasma wave in terms of a slowly varying, dimensionless, complex Langmuir wave envelope $\mathcal{E}(z,t)$ and carrier phase $\phi_2(z,t) = -k_2 z - \omega_2 t$ as

$$E_z(z,t) = \frac{m\omega_p^2}{ek_2\sqrt{2}}[\mathcal{E}(z,t)e^{-i(k_2 z+\omega_2 t)} + c.c.] \equiv \frac{m\omega_p^2}{ek_2\sqrt{2}}\mathcal{E}e^{i\phi_2} + c.c., \quad (2)$$

where the cold, linear plasma frequency $\omega_p$ is related to the (presumed uniform) equilibrium electron number density $n_0$ by $\omega_p^2 \equiv 4\pi e^2 n_0/m_e$. The central frequency and wave vector are given by the beating between the counter-propagating laser fields, so that $\omega_2 \equiv \omega_0 - \omega_1$ and $k_2 \equiv k_0 + k_1$, and we assume the laser frequencies are tuned so as to nearly match the natural Langmuir oscillation frequency: $\omega_2 = \omega_0 - \omega_1 \approx \omega_p$. The frequencies and wavenumbers of the laser carriers may be taken to satisfy either the usual linear dispersion relation $\omega_{0,1}^2 = \omega_p^2 + c^2 k_{0,1}^2$ in a cold but collisionless plasma, or else more simply, the vacuum dispersion relation $\omega_{0,1} \approx ck_{0,1}$, since the plasma is assumed underdense, in that $\omega_p \ll \omega_{0,1}$. All ion motion is neglected, while electron longitudinal motion in the plasma wave and transverse quiver motion in the laser fields are assumed to remain nonrelativistic.

The plasma response is driven ponderomotively by the beating of the counter-propagating lasers and, in turn acts as a source in Maxwell's equations. Retaining only the slowly varying, resonant parts of the transverse electromagnetic waves and the longitudinal plasma wave leads to the following three-wave equations (see, e.g., Ref. 7 for a more detailed derivation):

$$\left[\frac{\partial}{\partial t} - c\frac{\partial}{\partial z}\right]a_0 = \frac{ck_2\omega_p}{2\sqrt{2}\omega_0}a_1\mathcal{E}, \quad (3)$$

$$\left[\frac{\partial}{\partial t} + c\frac{\partial}{\partial z}\right]a_1 = -\frac{ck_2\omega_p}{2\sqrt{2}\omega_1}a_0\mathcal{E}^*, \quad (4)$$

$$\left[\frac{\partial}{\partial t} + i(\omega_L - \omega_2) + i\delta\omega + \nu\right]\mathcal{E} = -\frac{ck_2}{2\sqrt{2}}a_0 a_1^*. \quad (5)$$

Because of our assumption of an underdense plasma, note that here the laser envelopes have been assumed to advect at the vacuum group velocity $\pm c$. In the equations above we included not only the linear frequency difference (from the cold resonance), $\omega_L - \omega_2$, but also a nonlinear frequency shift $\delta\omega$ and a damping coefficient $\nu$ which are in general functionals of the local plasma wave excitation. As discussed in Ref. 8, assuming an initially Maxwellian electron plasma with 1D rms thermal velocity $v_{\text{th}}$, the linear frequency $\omega_L$ of the driven, growing Langmuir wave is given by the real part of the root of the Vlasov–Landau dispersion relation, which to leading order in $v_{\text{th}}k_2/\omega_p$ just reproduces the familiar Bohm–Gross thermal correction.

We use the nonlinear terms $\delta\omega$ and $\nu$ to model plasma kinetic effects such as Landau damping and particle trapping in the Langmuir wave, which we compute using the scheme described in Ref. 5. This model is based on the conservation of canonical particle action in the slowly growing plasma

wave and the observation that, after sufficiently many oscillations in the plasma wave, the trapped particles become almost uniformly distributed in the canonical phase angle conjugate to this action. Thus, the nonlinear Langmuir wave approximates a Bernstein–Greene–Kruskal (BGK)-type wave that is invariant in the canonical particle action. The process of phase mixing in the wave to produce this BGK-type state extracts energy from the wave; for small amplitude waves this is the familiar linear Landau damping. For larger amplitude waves the peak instantaneous damping rate $\nu_{\max}$ can be higher than the linear level, because significant numbers of particles can be trapped and accelerated in the wave.[9,10] However, this elevated damping rate typically occurs only for a short time, since the large amplitude wave quickly flattens the particle distribution to form the undamped BGK-like state.

Similar considerations using action conservation were also used by Bènisti and Gremillet[11] to develop a reduced kinetic plasma model. Our scheme differs in that we use a simple but heuristic method to determine how the kinetic plasma response (i.e., the nonlinear frequency shift $\delta\omega$ and damping $\nu$) will evolve from the initial state characterized by Landau damping and particle trapping to the asymptotic final state in which the electrons are phase mixed in the wave, resulting in an undamped BGK-type wave that has an associated nonlinear frequency shift. In the initial state, the damping is maximized at a level near $\nu_{\max}(|\mathcal{E}|)$ so as to, roughly speaking, dissipate an "incoherent" energy $U_{\text{incoh}}$ in a time of order one bounce oscillation in the wave, $\tau_B \sim 1/\omega_p\sqrt{|\mathcal{E}|}$, while the maximum nonlinear frequency shift $\delta\omega_{\max}(|\mathcal{E}|)$ is determined such that the invariant-in-action, BGK-type state self-consistently supports the electrostatic field of the Langmuir wave; for further details see Ref. 5. To transition between these two limits in a simple yet physically motivated manner, we note that the Langmuir wave energy that is extracted by the damping coefficient $\nu$ must be transferred to the kinetic energy of the individual particles as they phase mix in the wave. Comparing the cumulative (integrated) energy $U_{\text{damp}}$ damped due to $\nu$ to that required to produce the time-asymptotic BGK-type state, namely, $U_{\text{incoh}}$, provides an indirect measure for determining the degree of phase mixing, which in turn is used to determine the relative amount of damping and frequency shift via the ansatz,

$$\nu(|\mathcal{E}|,\Upsilon) = \nu_{\max}\Upsilon, \tag{6}$$

$$\delta\omega(|\mathcal{E}|,\Upsilon) = \delta\omega_{\max}(1-\Upsilon), \tag{7}$$

where, based on some numerical calibration, the smooth function $\Upsilon$ transitioning between the initial and completely phase-mixed limits is taken to be

$$\Upsilon = \frac{1}{2}\left\{1+\tanh\left[\frac{7}{2}\left(1-2\frac{U_{\text{damp}}}{U_{\text{incoh}}}\right)\right]\right\}, \tag{8}$$

where some numerical tests confirmed that results are not terribly sensitive to the precise form of this interpolation function.

Note that Eqs. (6)–(8) imply that the wave damping is assumed maximal when there has been insufficient time to develop the phase-mixed, BGK-type mode, while the damping almost vanishes and the nonlinear frequency shift is maximized when the amount of energy damped from the wave approaches that required to support the asymptotic distribution function. The instantaneous local bound $\delta\omega_{\max}$ on the detuning can in principle be of either sign, but when the actual nonlinear frequency shift is non-negligible (i.e., after phase mixing), it will satisfy $\delta\omega_{\max}<0$. Although the plasma wave nonlinearities are simply parametrized, given a forcing consisting of the superposition of the self-consistent laser fields, the interplay of the evolving detuning and damping and their effect on the growth of the Langmuir mode, and the feedback on the laser fields, can be complex.

Note that the parameters $\nu_{\max}$, $\delta\omega_{\max}$, and $U_{\text{incoh}}$ are functions of the local, instantaneous plasma wave amplitude $|\mathcal{E}(z,t)|$, as well as the equilibrium plasma density and temperature (via the plasma frequency $\omega_p$ and the Debye length $\lambda_D$). These parameters can be extracted (approximately) within the ETW theory, but for speed in actual numerical simulations they are first precalculated at needed plasma temperatures and densities over a sample of discrete Langmuir wave amplitudes covering the expected range, and then these data are stored in lookup tables and used to define simple polynomial or rational interpolating functions for any intermediate amplitudes. This avoids some costly numerical quadratures and root finding at each time step. The cumulative damped energies $U_{\text{damp}}$ are functionals of the plasma dynamics up to the current instant of time and are accumulated for each grid point during the numerical integration.

This specific ETW model has been incorporated into an ANSI C code dubbed THWACK, for THree-Wave with Action-Conserving Kinetics, which includes some specialized numerical features in addition to the lookup tables used to efficiently infer the detuning and damping terms. Because the three-wave equations are notoriously prone to numerical instabilities when advanced by standard finite difference algorithms, instead we adopt an operator-splitting approach, which enjoys many advantages. The evolution of all three modes is absolutely stable numerically for any choice of time step, there is no spurious linear dispersion in the advection of the lasers, and in the limit of vanishing thermal and kinetic effects, a discrete version of the Manley–Rowe (local wave action conservation) relations will be exactly preserved.

Similar models that interpolate between an initially damped state and an asymptotic one characterized by a nonlinear frequency shift were previously proposed in Refs. 12–14; ours differ by using the calculated properties of the invariant-in-action, BGK-type state to determine the damping, frequency shift, and the manner by which to transition between them. An alternative reduced kinetic based on quasilinear theory was recently developed in Ref. 15 and applied to study PBRA in Ref. 16.

Having described the properties of our ETW model, we proceed to use this model to simulate an example of PBRA in one dimension and compare its performance with that of PIC code, as well as to a more conventional "Landau" three-wave (LTW) model which includes the familiar linear

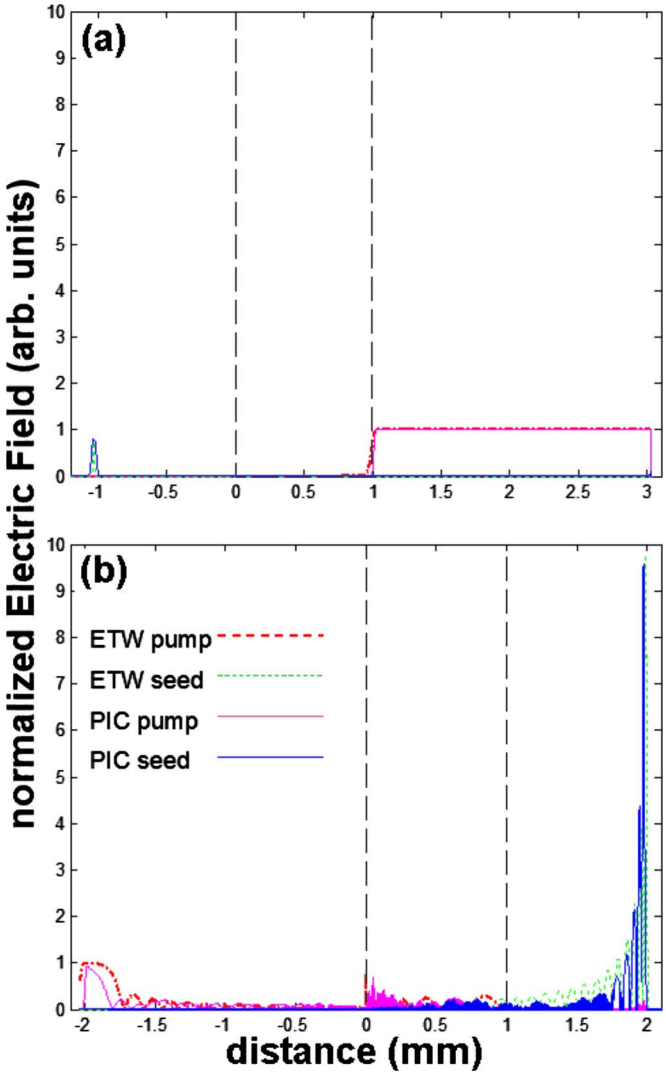


FIG. 1. (Color online) Snapshots of the 1054 nm pump laser envelope and the 1300 nm seed laser envelope interacting in a cold plasma (a) near the beginning of the simulations, with the seed still outside the plasma and the pump just entering the plasma and (b) near the end of the simulations, after the bulk of the seed and pump envelopes have exited the plasma. In (b) the dashed line on the left hand side is the ETW pump and the solid line is the PIC pump. The dashed line on the right hand side is the ETW seed and the solid line is the PIC seed. The vertical dashed lines indicate the boundaries of the 1 mm plasma slab; refer to the text for the other parameters of this simulation.

Bohm–Gross-like detuning in and linear Landau damping of the plasma wave but no nonlinear kinetic effects, simulated using the same THWACK code with appropriate settings.

## III. 1D PBRA CASE STUDY OF ETW AND LTW VERSUS PIC

For this comparison, we compared results of the ETW and simpler LTW models as implemented in the THWACK code to those of the 1D version of the fully kinetic PIC code OSIRIS.[17] The parameters chosen in these simulations are very similar to those in the work of Clark and Fisch.[18] In this setup we specify a 1 mm uniform plasma with a density of $3.6\times10^{19}$ cm$^{-3}$, buffered by vacuum regions on both sides. As shown in Fig. 1 for a cold plasma, the 1054 nm pump laser envelope travels from right to left while the 1300 nm seed laser envelope propagates from left to right. The 1300 nm vacuum wavelength for the seed carrier is chosen so that the difference between the corresponding pump and seed frequencies is the cold linear plasma frequency. The vacuum regions are wide enough to contain the entire pump and seed after they leave the plasma slab, allowing diagnostic "observation" of the laser pulses in vacuum outside of the plasma. The pump is specified as having $a_0=0.015$ with a 100 fs rise followed by a 6.66 ps flat top. The seed is specified as an approximate Gaussian having $a_1=0.015$ with a pulse width of 100 fs. For the PIC simulations, the box size is $3.025\,045\times10^4 c/\omega_0$ and contains $2.900\,00\times10^5$ uniform cells with 128 macroparticles per cell. Length units are normalized to $c/\omega_0$(0.17 $\mu$m) and time units are normalized to $1/\omega_0$ (0.56 fs) for the 1054 nm pump laser. The time step used is 0.058 fs and the total simulation time is 13.6 ps. The cell size is $0.1043c/\omega_0$, corresponding to 60 cells per pump laser wavelength. The ions are taken as fixed, so only the electron sheets are allowed to move.

TABLE I. Parameters for the three-wave models ($\omega_L$ is the linear Langmuir wave frequency and $\lambda_D$ is the Debye length).

| | Temperature (eV) | $k_2\lambda_D$ | $\omega_L/\omega_p$ |
|---|---|---|---|
| (a) | 0 | 0 | 1 |
| (b) | 78 | 0.115 | 1.02 |
| (c) | 142 | 0.156 | 1.038 |
| (d) | 200 | 0.185 | 1.055 |
| (e) | 365 | 0.25 | 1.106 |
| (f) | 525 | 0.3 | 1.158 |

Upon looking at the test case presented in Fig. 1, we observe reasonably close overlap between ETW/LTW and PIC predictions for the seed and pump envelopes at the beginning and at the end of the simulation in the case of a cold plasma, i.e., with thermal effects suppressed in the ETW or LTW models (which therefore coincide) and with a cold start utilized in the PIC simulations.

Having verified reasonable agreement between the three-wave and PIC algorithms for a cold plasma, we next examine predictions for a thermal plasma. We compared results at a sequence of initial plasma temperatures corresponding to 78, 142, 200, 365, and 525 eV, all with the same initial pump and seed lasers. Because of thermal effects, the linear resonant plasma frequency $\omega_L$ is modified from the cold plasma frequency $\omega_p$, and thus for higher temperatures the resonance between the lasers and the plasma becomes increasingly detuned. As mentioned previously, the code makes use of an interpolating functions based on lookup tables which are derived from the ETW model for each temperature and corresponding $\omega_L$ value for the chosen plasma density. Table I provides these basic parameters for each of the temperature cases. The LTW included the real (detuning) and imaginary (damping) frequency shifts of the Langmuir wave as predicted from linear theory via the Vlasov–Landau dispersion relation, but none of the additional nonlinear kinetic physics incorporated in the ETW model.

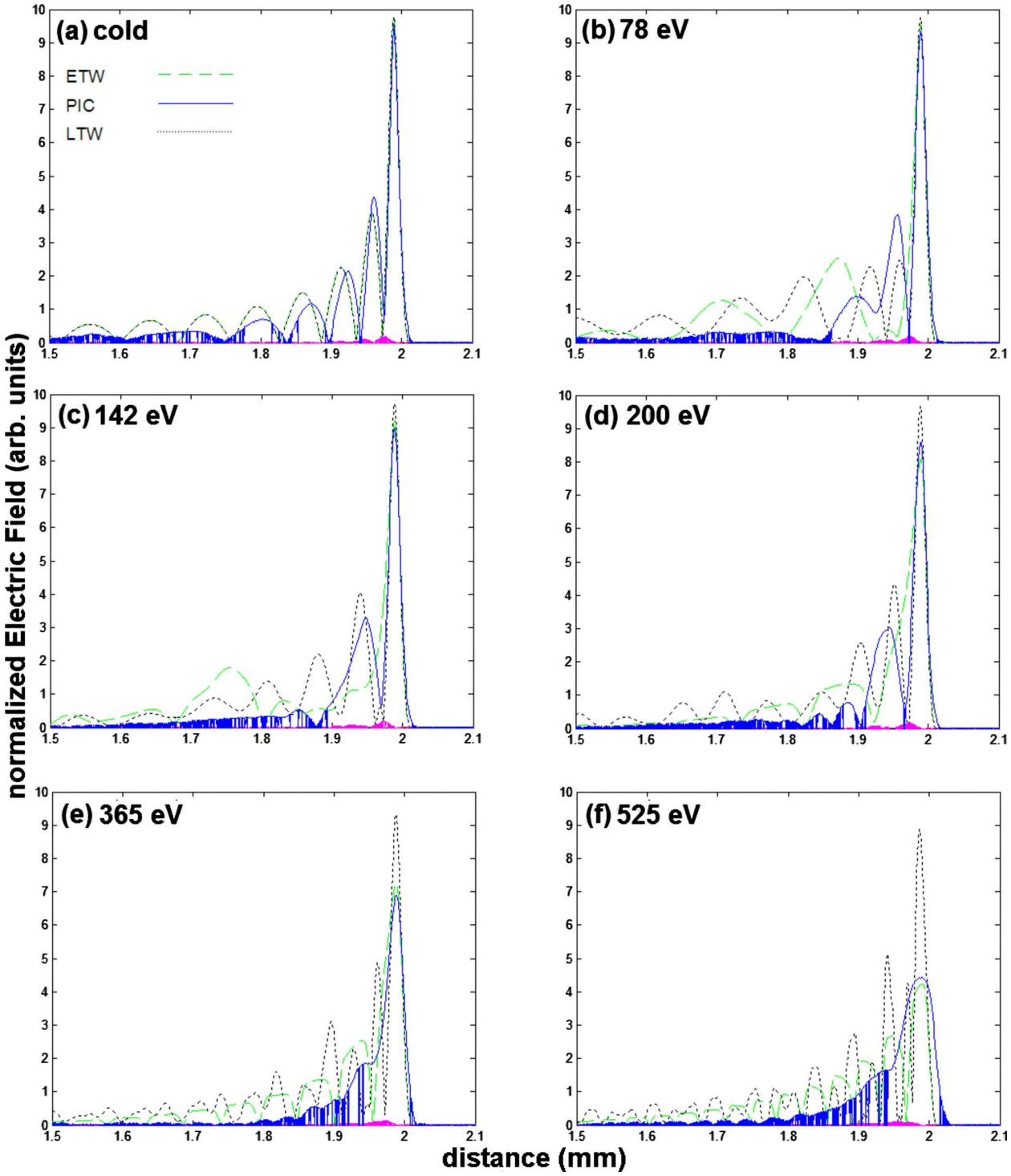


FIG. 2. (Color online) Profiles of the final seed laser envelopes (dashed for ETW, solid for PIC, dotted for LTW) after exiting the plasma for (a) cold, (b) 78 eV, (c) 142 eV, (d) 200 eV, (d) 365 eV, and (e) 525 eV cases. Due to the difference in group velocities, the PIC waveforms have been shifted to best overlap with the three-wave envelopes. The fine-scale spikiness in the PIC seed is due primarily to numerical errors in the simple algorithm employed to approximate the envelope from the full transverse electric fields, while the remnant traces of the counter-propagating fields are a numerical artifact of the directional diagnostic used to extract the left and right-moving modes of the EM fields on a staggered Yee grid.

The results of the comparison between the ETW, LTW, and PIC codes for the seed pulse in each of the thermal plasma simulations are shown in Fig. 2, which zooms in on a local section of the simulation box containing the first few peaks of the seed envelopes. The previous cold plasma simulation result is also included for reference. Since amplitudes in the three-wave simulations are normalized to the initial pump amplitude, the PIC result was scaled in the same manner in order to overlap meaningfully the three-wave and PIC predictions. Note that because the three-wave models as implemented advect the laser fields precisely at speed $c$ while the PIC propagates the laser fields at something closer

to $v_{g_{1,2}}=c[1-\omega_p^2/\omega_{0,1}^2]^{1/2}$ while inside the plasma, a slight overall phase shift of the PIC waveforms was introduced in order to compensate for the differing group velocities and observe the best-case overlap.

Upon performing these phase shifts to adjust for differences in group delay, we can observe reasonably good agreement between ETW and PIC results for all cases (a)–(f), which generally improves as the temperature decreases. Furthermore, at sufficiently low temperatures, the final seed in the ETW model does resemble to some extent the characteristic self-similar $\pi$-pulse structure described in the nonlinear theory of PBRA for amplified seed pulses.[3,4] The agreement between PIC and ETW is clearly best in the leading spike of the seeds, where the peak amplitudes and pulse widths match reasonably closely at low temperatures and still moderately well at higher temperatures.

Taking the PIC results as our best guess of the "true" fields (i.e., the fields that would be predicted by the full Vlasov–Maxwell theory), the ETW and LTW results necessarily coincide at zero temperature, but increasingly diverge as the temperature is increased. At the lower temperatures, the leading spikes have temporal widths of $O(50$ fs) at half maximum and $O(100$ fs) near the base, while the bounce period is estimated as $O(25$ fs). Therefore, even at lower (but nonzero) temperatures, a given plasma particle may execute a significant fraction of one bounce oscillation or more while under the leading spike of the seed envelope, so we should not be surprised that the predictions of the ETW and LTW models begin to differ. Overall, the ETW model performs as well as or better than the LTW model, except that at low temperatures the width of the first spike appears to be slightly better predicted by the LTW model. Both the ETW and LTW tend to misrepresent the width of the leading spike at higher temperatures, but for warmer plasmas, the LTW model begins to underestimate the width more than the ETW model, and also consistently overestimates the height of the leading spike compared to the predictions of the ETW model, by significant amounts at the higher temperatures.

Compared to PIC, both three-wave models tend to overestimate the "coherence" in the tail of the amplified seed envelope, in that they predict too many discernible secondary spikes of too high contrast, or visibility. At lower temperatures, accuracy of the ETW and LTW prediction in the trailing portion of the seed might be described as a wash, but at higher temperatures, the ETW model does better in the sense of predicting fewer discernible secondary spikes and tracking somewhat more closely the general decay of the amplitudes.

Because agreement between PIC and ETW is reasonably close in the leading spike of the seeds, in terms of both peak amplitudes and pulse widths, we expect that their predictions for two observables of practical interest, namely, peak intensity and total energy in the leading spike, should also compare favorably, remaining well within the same order-of-magnitude over the covered temperature range. To quantify this further, Fig. 3 shows a plot of normalized peak seed intensity in the eikonal approximation versus time and compares the ETW to the LTW and PIC results.

From the figure, we are reassured that in no case does amplification occur unless the seed and pump overlap inside the plasma, and we observe, as would be expected, that the PIC and three-wave models tend to agree better at lower temperatures. The ETW models underestimate the peak intensity achieved at all but the highest temperature considered, but at moderate temperatures (up to 200 eV) the predicted peak seed intensities in the ETW and PIC differ by no more than 10%, and even at the higher temperatures, they agree to within 20%. In contrast, the LTW model always overestimates the peak power, with this error becoming increasingly pronounced at higher temperatures. At the highest temperature, the LTW result overestimates the PIC result by about 300%.

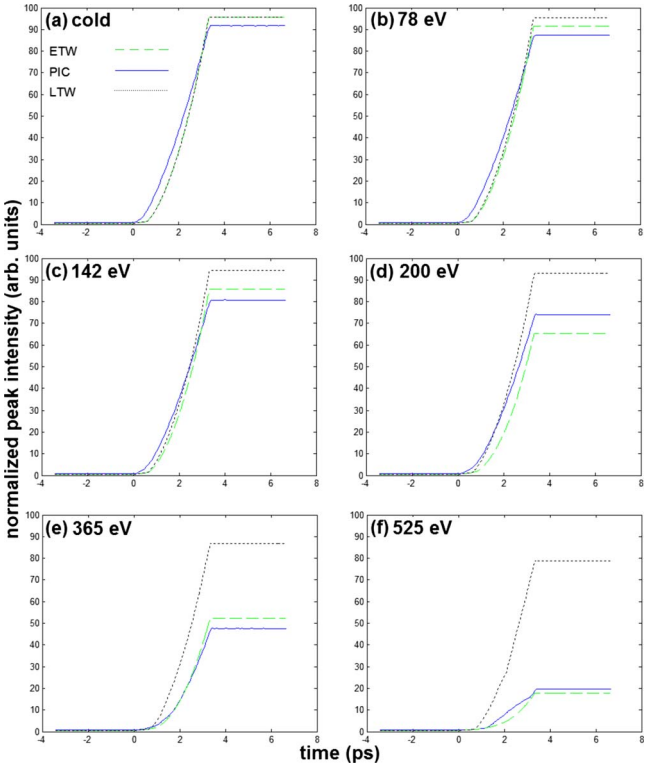


FIG. 3. (Color online) Time series of normalized peak intensity vs time for (a) cold, (b) 78 eV, (c) 142 eV, (d) 200 eV, (d) 365 eV, and (e) 525 eV cases, showing predictions of the ETW (dashed), PIC (solid), and LTW (dotted) models. At time $t=0$ ps the peak of the seed and the peak of the pump meet close to the leading (left) edge of the plasma slab.

From examination of the plots, we also note that the growth rates for the ETW seed and the PIC seed are quite similar as they deplete the pump and become amplified inside the plasma, although some differences in the onset times of the nonlinear PBRA regimes are evident, so that the overall amplifications at a given time are somewhat different.

In all, agreement between ETW and PIC is generally superior to that between LTW and PIC. Efforts are underway to pinpoint the exact cause of increasing discrepancy between ETW and PIC for higher temperature regimes and to resolve residual disagreement over the peak intensities. Furthermore, as visual inspection of the seed envelopes in Fig. 2 revealed, rather different waveform features emerge in the secondary pulselets behind the leading spike, where wave action and energy are traded back and forth between seed, pump, and plasma, with some energy "leaking" into the in-

coherent particle motion. Further simulations must be done to ascertain the causes of these differences in trailing edge behavior.

In this preliminary study, we merely point out that the ETW model was neither designed nor expected to function accurately at arbitrarily high temperatures (nor should its results be trusted at very low temperatures, where the neglected effects of Coulomb collisions would become important). Although the ETW model takes certain kinetic effects into account, it does not comprehensively include all the kinetic physics, most notably full wave breaking of the plasma wave and nonlinear saturation of the seed growth in PBRA. In addition, the ETW model presumes sufficiently slow growth and/or Landau damping of the plasma wave so that adiabatic invariance of electron motion is maintained. Obviously violations of adiabaticity assumptions may impact the performance of the ETW model. For that matter, it is not obvious that the present PIC simulations offer completely reliable benchmarks at the highest temperatures, because convergence runs for the PIC simulations were performed at an intermediate temperature, and as the temperature is increased, additional macroparticles per cell may be needed to resolve the tails of the electron velocity distribution function. In particular, it is not yet certain whether the predictions of the PIC model in the trailing edge of the seed are entirely accurate, reflecting additional warm wave breaking or other thermal-kinetic effects not incorporated into the ETW model, or whether the observed decoherence is perhaps being exacerbated by numerical heating.

Thus we should not be overly surprised or disappointed by the differences in quantitative detail between the ETW and PIC results. Nonetheless, the ETW model used in this study of PBRA is an improvement over either ordinary (cold and undamped) three-wave models or the LTW model, in that it incorporates important nonlinear aspects of the most important kinetic effects, and its modeling capability agrees with PIC-based Vlasov–Maxwell simulations to a certain qualitative and semiquantitative extent, while enjoying the virtues of computational simplicity and speed. The time required to integrate typical cases with the ETW code was vastly shorter, by two or three orders-of-magnitude or more, than that required for the corresponding case simulated using the PIC code. For example, the same case study that took less than one minute on a dual-core Intel PC running the THWACK code implementing the ETW model required approximately 13 h on 32 processors of a parallel supercomputing cluster running the 1D OSIRIS PIC code.

## IV. DISCUSSION

We sought to make a preliminary assessment of the power and limitations of a recently proposed 1D reduced model of nonlinear Raman Backscatter (RBS) or similar laser-plasma interactions in underdense, moderately thermal plasmas. The ETW model achieves computational simplicity and efficiency by using a highly reduced description of the plasma dynamics in comparison to the full Vlasov–Maxwell equations, but retains higher accuracy over standard reduced descriptions such as fluid models, the cold three-wave model, or even the LTW that includes linear damping and detuning, by incorporating true nonlinear kinetic effects.

We compared the simple-but-efficient ETW model to an even simpler LTW model and a more complete but time-consuming PIC code in the specific context of studying the dynamics of the PBRA in one spatial dimension. We found reasonably good agreement between the ETW and PIC for thermal plasmas at moderate temperatures, i.e., with $k\lambda_D \lesssim 0.25$, or even somewhat larger, while the LTW model significantly overestimates peak intensity in the amplified seed pulse as the initial plasma temperature is increased.

Because the ETW code runs significantly faster and yet can still produce similar results to that of a 1D PIC code over some moderate range of temperatures, our study has shown that the ETW description can be an efficient and viable modeling tool for studying the PBRA problem in 1D thermal plasmas, especially when computational efficiency is paramount, although there are persistent discrepancies in the trailing portion of the amplified seed and increasing discrepancies at higher temperatures which should be studied further.

Since for typical parameters and geometries of interest the ETW equations can be integrated very efficiently, this model may potentially be employed for doing extensive parameter scans in order to identify promising regimes of interest that can be studied further using more accurate simulations via PIC or otherwise followed up by different means. It is also practical to use the ETW algorithm to simulate PBRA scenarios involving much longer plasmas and therefore larger interaction lengths[19] that would require unreasonable computational resources if performed using PIC codes.

In assessing the utility of the ETW model, one should remain mindful not only of the usual and inevitable accuracy-versus-speed tradeoffs, but also more generally of the roles played by 1D models in laser-plasma theory and simulation. 1D models are not (or at least, should not) be used with the expectation of obtaining very precise quantitative predictions, for real experiments are performed in a three-dimensional world, and too much transverse physics is inevitably left out of even our best 1D models—diffraction, filamentation, return currents, inhomogeneities, additional instabilities, etc.—to reasonably expect close agreement with more complete descriptions (or, of course, with actual experimental measurements). However, 1D models can be efficient and powerful tools to establish preliminary proofs-of-principle for new ideas or configurations, or to perform parameter searches or other exploratory analyses in order to find promising regimes in which to then subsequently expend limited computational resources on more detailed, if demanding, higher-dimensional simulations. Our preliminary comparisons suggest that the ETW model may offer a good compromise between computational efficiency and physical accuracy for the legitimate simulations purposes to which such a reduced model may be applied.

In closing, we also point out that the physics and numerics that underlie our ETW model are the result of one particular approach to expand the framework of ordinary three-wave models, so as to more accurately account for the actual kinetic behavior of thermal plasmas. The ETW model is

similar in some respects to recent work done by other authors, particularly the use of interpolation between damped and phase-mixed dynamical states of the plasma,[12–14] and the central role played by canonical particle action.[11] Recently, Fisch *et al.*[15,16] proposed an alternate approach[15,16] based on quasilinear theory that addresses the same goals over similar parameter regimes. A distinct "envelope-kinetic" numerical model incorporating certain algorithmic techniques from both PIC codes and FEL simulations[20] has been applied to the PBRA problem by Hur *et al.*[21] Clearly there is interest in the continual development of extensions or generalizations of three-wave models in the context of backward Raman amplification or other laser-plasma interactions. Future work will likely center on more careful comparisons and assessment of these various schemes, and further extensions to allow for higher temperatures or to incorporate multidimensional geometry,[22,23] or additional mechanisms that in real-world experiments contribute to the detuning from resonance, such as frequency chirping of the lasers or gradients or inhomogeneities in the plasma density.

## ACKNOWLEDGMENTS

This work was supported by the Lawrence Livermore University Education Partnership Program, by the U.S. Department of Energy (DOE), Grant No. DE-FG02-04ER41289, and by the NNSA under the SSAA Program through U.S. DOE Research Grant No. DE-FG5207NA28122. We thank W. B. Mori for the use of the OSIRIS code for conducting this comparative study.

[1] C. K. Birdsall and A. B. Langdon, *Plasma Physics via Computer Simulation* (IOP, Philadelphia, 1991).
[2] G. Shvets, N. J. Fisch, A. Pukhov, and J. Meyer-ter-Vehn, Phys. Rev. Lett. **81**, 4879 (1998).
[3] V. M. Malkin, G. Shvets, and N. J. Fisch, Phys. Rev. Lett. **82**, 4448 (1999).
[4] V. M. Malkin, G. Shvets, and N. J. Fisch, Phys. Rev. Lett. **84**, 1208 (2000).
[5] R. R. Lindberg, A. E. Charman, and J. S. Wurtele, Phys. Plasmas **15**, 055911 (2008).
[6] R. R. Lindberg, A. E. Charman, and J. S. Wurtele, Phys. Plasmas **14**, 122103 (2007).
[7] W. L. Kruer, *Physics of Laser Plasma Interactions* (Westview, Boulder, 2003).
[8] H. A. Rose and D. A. Russell, Phys. Plasmas **8**, 4784 (2001).
[9] R. Sugihara and K. Yamanaka, Phys. Fluids **18**, 114 (1975).
[10] N. S. Bulechelnikova and E. P. Matochkin, Sov. J. Plasma Phys. **6**, 1057 (1980).
[11] D. Bénisti and L. Gremillet, Phys. Plasmas **14**, 042304 (2007).
[12] E. A. Williams, B. I. Cohen, L. Divol, M. R. Dorr, J. A. Hittinger, D. E. Hinkel, A. B. Langdon, R. K. Kirkwood, D. H. Froula, and S. H. Glenzer, Phys. Plasmas **11**, 231 (2004).
[13] H. X. Vu, D. F. DuBois, and B. Bezzerides, Phys. Plasmas **14**, 012702 (2007).
[14] B. I. Cohen, E. A. Williams, and H. X. Vu, Phys. Plasmas **14**, 102707 (2007).
[15] N. A. Yampolsky and N. J. Fisch, Phys. Plasmas **16**, 072104 (2009).
[16] N. A. Yampolsky and N. J. Fisch, Phys. Plasmas **16**, 072105 (2009).
[17] R. A. Fonseca, L. O. Silva, F. S. Tsung, V. K. Decyk, W. Lu, C. Ren, W. B. Mori, S. Deng, S. Lee, T. Katsouleas, and J. C. Adam, Lect. Notes Comput. Sci. **2331**, 342 (2002).
[18] D. S. Clark and N. J. Fisch, Laser Part. Beams **23**, 101 (2005).
[19] R. K. Kirkwood, E. Dewald, C. Niemann, N. Meezan, S. C. Wilks, D. W. Price, O. L. Landen, J. Wurtele, A. E. Charman, R. Lindberg, N. J. Fisch, V. M. Malkin, and E. O. Valeo, Phys. Plasmas **14**, 113109 (2007).
[20] M. S. Hur, R. R. Lindberg, A. E. Charman, J. S. Wurtele, and H. Suk, Phys. Rev. Lett. **95**, 115003 (2005).
[21] M. S. Hur, S. H. Yoo, and H. Suk, Phys. Plasmas **14**, 033104 (2007).
[22] A. A. Balakin, G. M. Fraiman, and N. J. Fisch, IEEE Trans. Plasma Sci. **33**, 488 (2005).
[23] G. Fraiman, N. A. Yampolsky, V. M. Malkin, and N. J. Fisch, Phys. Plasmas **9**, 3617 (2002).